ISSN (Print) 1226-1750
ISSN (Online) 2233-6656
Journal of Magnetics 30(4), 758-763 (2025) https://doi.org/10.4283/JMAG.2025.30.4.758

Evaluation of X-ray Attenuation Characteristics of 3D Printed Thermoplastic Slabs for Phantom Replacement Application

Kyung-Hwan Jung[1], Ki-Yoon Lee[1], Hyun-dong Kim[1], Jang-Oh Kim[2], Chang-Ho Lee[3], and Cheol-Ha Baek[4]*

[1]*Department of Medical Health Science, Kangwon National University, Samcheok 25949, Republic of Korea*
[2]*Department of Radiological Science, Inje University, Gimhae 50834, Republic of Korea*
[3]*Department of Emergency and Disaster Management, Inje University, Gimhae 50834, Republic of Korea*
[4]*Department of Radiological Science, Kangwon National University, Samcheok 25949, Republic of Korea*

(Received 29 October 2025, Received in final form 23 December 2025, Accepted 23 December 2025)

This study quantitatively investigated the attenuation characteristics of 3D printed thermoplastic materials under electromagnetic radiation in the diagnostic energy range to evaluate their feasibility as substitutes for the conventional phantom material, polymethyl methacrylate (PMMA). Slabs fabricated from polylactic acid (PLA) and acrylonitrile–butadiene–styrene (ABS) were examined at equivalent beam energies corresponding to tube potentials of 50, 70, and 100 kVp, with thicknesses of 5, 10, and 15 mm and infill densities of 20%, 60%, and 100%. Both experimental measurements and Monte Carlo simulations using MCNP 6.3 were performed. The average discrepancy between simulation and experiment was within 2.3%, indicating excellent agreement. Compared with PMMA, the mean attenuation differences for PLA and ABS were 3.7% and 8.8%, respectively. The penetrated dose increased linearly as the infill density decreased due to a reduction in effective density caused by higher porosity. PLA exhibited attenuation behavior nearly identical to PMMA because of its similar density and effective atomic number, which governs the electromagnetic interaction behavior, whereas ABS showed higher penetration, suggesting potential use as a lightweight structural support material. These results demonstrate that 3D printed thermoplastics provide sufficient quantitative reliability to serve as alternative phantom materials and can be effectively applied to patient-specific phantom fabrication and quality assurance (QA) or quality control (QC) procedures in diagnostic and therapeutic imaging systems.

Keywords : 3D printing, thermoplastic materials, electromagnetic radiation, Monte Carlo simulation, electromagnetic interaction

1. Introduction

Medical imaging plays an essential role in disease diagnosis, treatment planning, and in the quality control (QC) and quality assurance (QA) of imaging systems [1, 2]. To ensure image reliability and patient safety, quantitative evaluations using tissue-equivalent phantoms that simulate the attenuation characteristics of human tissues to electromagnetic radiation are required [3]. Accordingly, the American College of Radiology (ACR) and the American Association of Physicists in Medicine (AAPM) recommend standardized phantoms for CT, MRI, ultrasound, and PET systems to evaluate geometric accuracy, slice thickness, contrast resolution, and image uniformity [4, 5]. Commercially available phantoms, however, have several limitations. Most of them are fabricated from polymethyl methacrylate (PMMA) or other polymeric materials, which are costly and optimized for specific devices or purposes, making them difficult to modify or customize [6]. Moreover, they do not fully reproduce the physical and radiological properties of diverse human tissues, restricting their use in patient-specific or multimodality imaging [7]. Recently, additive manufacturing (AM), also known as 3D printing, has been introduced as an alternative solution to overcome these issues [8]. This technique can reproduce complex anatomical structures from digital medical imaging data at low cost and high precision. Furthermore, material composition, internal infill density, and structural pattern can be controlled to achieve tissue equivalency [9, 10]. Qiu et al. developed a multimodal phantom applicable to both CT and MRI using 3D printing [11], while Kunert et

*Corresponding author: Tel: +82-33-540-3384
e-mail: baekch@kangwon.ac.kr

al. confirmed the high correlation between measured CT doses and Monte Carlo simulations using a 3D printed pregnant phantom [12]. Nevertheless, most previous studies were conducted using PMMA at a single energy level of electromagnetic radiation, typically corresponding to an X-ray tube voltage of 120 kVp. Thus, quantitative data on the attenuation behavior of 3D printed materials under different diagnostic energy spectra remain insufficient [13]. Without validation under variable energy conditions and infill densities, the application of 3D printed phantoms as substitutes for commercial ones remains limited. This study compared the attenuation properties of commonly used thermoplastic materials with those of PMMA under electromagnetic radiation in the diagnostic energy range. Both experimental measurements and Monte Carlo simulations were performed to analyze dose variations according to material thickness and beam energy. In addition, attenuation changes depending on infill density were investigated to evaluate the cost-effectiveness and fabrication efficiency of 3D printed phantoms.

2. Materials and Methods

2.1. Experimental Setup for Evaluating X-ray Attenuation Characteristics of 3D Printed Slabs

To quantitatively evaluate the X-ray attenuation characteristics of 3D printed thermoplastic materials, experimental measurements were conducted by varying slab thickness and internal infill density. The experiment aimed to verify whether 3D-printed materials can reproduce tissue-equivalent attenuation behavior comparable to that of the conventional phantom material, PMMA. All slabs were fabricated using a fused deposition modeling (FDM) 3D printer (K1C, Creality, China), which is commonly used for thermoplastic filament printing. The test materials were selected as polylactic acid (PLA) and acrylonitrile butadiene styrene (ABS), which possess physical properties similar to those of PMMA typically used in medical imaging phantoms. The physical parameters of each material are detailed in Table 1.

As represented in Fig. 1, each slab was printed in a flat-plate geometry with dimensions of 100 × 100 mm². Three different thicknesses, 5 mm, 10 mm, and 15 mm, were fabricated, with the 5 mm slab serving as the reference

Fig. 1. (Color online) PLA and ABS slabs (5 mm thickness, 100% infill) fabricated by FDM 3D printing for X-ray attenuation measurements.

configuration, to compare attenuation performance. Then, to evaluate the effect of density variation on penetrated dose, the internal infill density was adjusted to 20%, 60%, and 100% using a rectilinear pattern, as illustrated in Fig. 2. The slab size for infill variation was 100 × 100 × 6 mm³. All slabs were designed to maintain a constant outer wall thickness so that only the internal structure varied among the test conditions.

X-ray irradiation experiments were performed using a diagnostic X-ray generator (ECO-CM-N, DRTECH, Korea). Tube voltages of 50 kVp, 70 kVp, and 100 kVp were selected for the measurements. The source-to-image distance (SID) was fixed at 100 cm, with the X-ray central axis aligned perpendicularly to the detector surface. Penetrated X-ray doses were measured using a MagicMax Multidetector (IBA, Germany). For each condition, the measurement was repeated five times, and the mean value was calculated to minimize statistical uncertainty. The penetration rate of each slab was then determined from the ratio of the penetrated dose to the incident dose.

2.2. Dose Comparison Using Monte Carlo Simulation

Monte Carlo simulations were performed using Monte Carlo N-Particle (MCNP) version 6.3 to reproduce the same geometric configuration as in the experimental

Table 1. Comparison of Physical and Radiological Properties of PMMA, PLA, and ABS.

Property	PMMA	PLA	ABS
Chemical formula	$(C_5O_2H_8)n$	$(C_3H_4O_2)n$	$(C_8H_8C_4H_6C_3H_3N)n$
Density (g/cm^3)	1.12±0.02	1.21±0.02	1.01±0.02
Average atomic number ($\bar{Z}$)	6.2	6.0	6.4

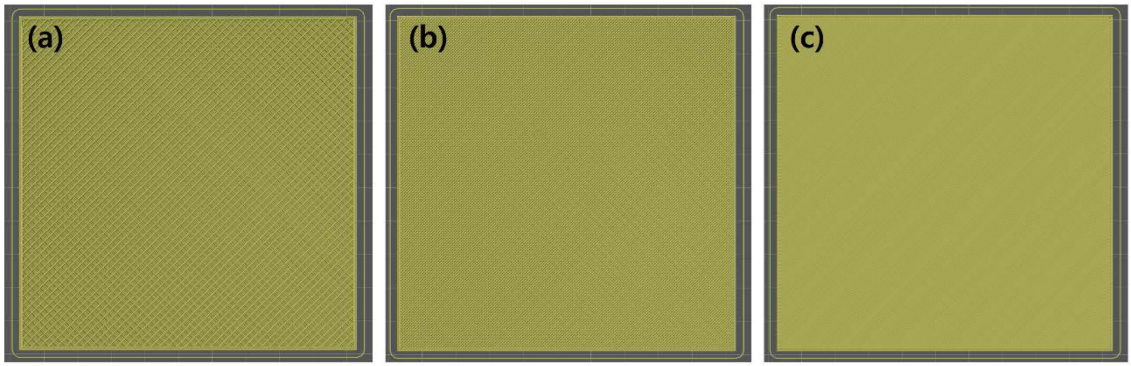

Fig. 2. (Color online) Internal patterns of 3D printed slabs with linear infill structures: (a) 20% infill, (b) 60% infill, and (c) 100% infill.

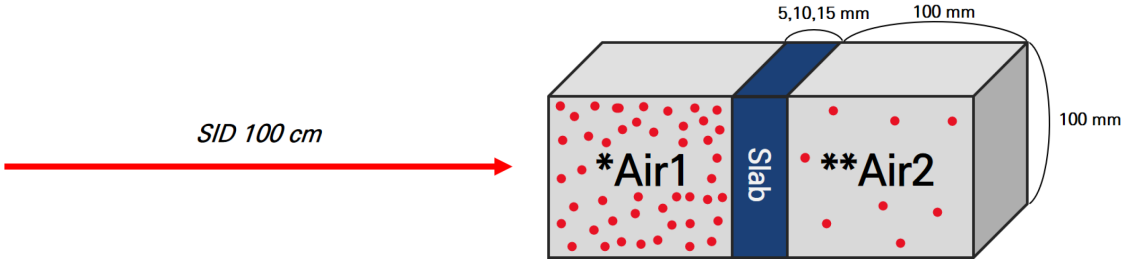

Fig. 3. (Color online) Schematic diagram of the MCNP simulation geometry representing X-ray attenuation through the 3D printed slab.

setup. As depicted in Fig. 3, the model consisted of a three-layer structure of air–slab–air to calculate the penetrated X-ray dose [14]. The lateral size of each slab was set to 100 × 100 mm², and the slab thickness was modeled as 5 mm, 10 mm, and 15 mm, identical to the experimental conditions.

The X-ray spectra were generated using the SRS-78 program by considering the filtration conditions of the diagnostic X-ray generator. Under an equivalent filtration of 1.2 mm Al, spectra corresponding to tube voltages of 50 kVp, 70 kVp, and 100 kVp were calculated, as graphed in Fig. 4. These spectra were then applied to the photon source definition in the Monte Carlo simulation [15].

The number of photons in each simulation was set to 1 × 10^8 to maintain a statistical uncertainty below 1%. The penetrated dose was calculated using the F4 (flux tally) option, which provides the average photon flux per unit volume. Based on these results, the effects of slab thickness and internal structure on X-ray attenuation were quantitatively analyzed and compared with the experimental measurements under the same tube voltage conditions.

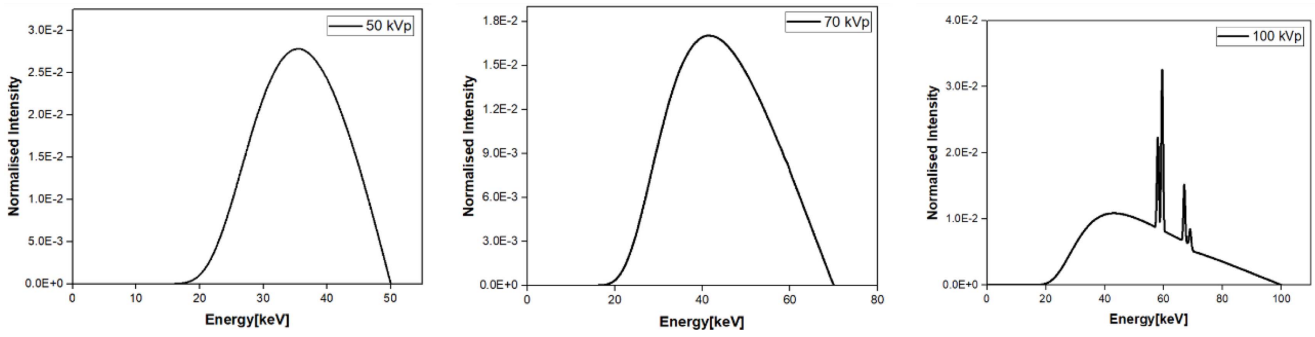

Fig. 4. X-ray energy spectra generated by the SRS-78 program for tube voltages of 50 kVp, 70 kVp, and 100 kVp.

3. Results and Discussion

This study evaluated the X-ray attenuation characteristics of PMMA, PLA, and ABS at diagnostic tube voltages of 50 kVp, 70 kVp, and 100 kVp, focusing on variations in slab thickness and internal infill density. The calculated doses were compared with the measured values, as summarized in Table 2, to verify the reliability of the Monte Carlo simulation. The results revealed that the penetrated dose decreased exponentially for both PLA and ABS as slab thickness increased at all tube voltages. Under the 50 kVp condition, the simulated doses for PLA were 248.0 μGy, 214.2 μGy, and 187.3 μGy at 5 mm, 10 mm, and 15 mm, respectively, while the measured doses were 242.1 μGy, 204.1 μGy, and 172.7 μGy. The corresponding relative errors were 2.38%, 4.72%, and 7.72%, with an average error of 4.96%. For ABS, the discrepancies between simulation and measurement were 0.12%, 0.79%, and 0.15%, yielding an average deviation of 0.35%. At 70 kVp, the simulated doses for PLA were 534.2 μGy, 470.6 μGy, and 421.4 μGy, whereas the measured values were 523.3 μGy, 455.5 μGy, and 398.6 μGy, resulting in errors of 2.04%, 3.21%, and 5.41% and an average deviation of 3.55%. For ABS, the simulated doses were 547.0 μGy, 495.4 μGy, and 450.6 μGy, while the measured doses were 551.1, 501.6, and 457.2 μGy. The corresponding differences were 0.75%, 1.25%, and 1.47%, with an average deviation of 1.16%. At 100 kVp, the simulated doses for PLA were 1092.9 μGy, 987.8 μGy, and 898.3 μGy, while the measured values were 1075.0 μGy, 963.7 μGy, and 863.2 μGy. The relative errors were 1.64%, 2.44%, and 3.91%, and the average difference was 2.66%. For ABS, the simulated doses were 1110 μGy, 1020 μGy, and 937 μGy, whereas the measured values were 1117 μGy, 1032 μGy, and 954.7 μGy. The deviations were 0.64%, 1.14%, and 1.89%, giving an average difference of 1.22%. When all tube voltage conditions were considered together, the overall mean discrepancy between measurement and simulation was approximately 2.3%, confirming the reliability of the Monte Carlo model. The reduction in error for PLA with increasing tube voltage can be attributed to the shift in dominant interaction mechanisms. At low energies, photon absorption is mainly governed by the photoelectric effect, which is highly sensitive to density and atomic number (Z). As tube voltage increases, the contribution of high-energy photons becomes significant, leading to the dominance of Compton scattering. This energy-dependent behavior was consistent with data from the NIST XCOM database, which reported mass attenuation coefficients (μ/ρ) of 0.1599 cm^2/g, 0.1565 cm^2/g, and 0.1596 cm^2/g for PMMA, PLA, and ABS, respectively [16]. These results emphasize that the attenuation characteristics of the three materials are nearly identical. Particularly, ABS maintained a deviation of less than 1% across all energy levels, demonstrating stable attenuation behavior as a homogeneous-density material.

Based on the validated simulation results, the penetrated X-ray doses of PLA and ABS were compared with those of PMMA to evaluate the physical equivalence of their attenuation characteristics. At 50 kVp, the relative differences of PLA from PMMA were 0.94%, 1.52%, and 2.52% for slab thicknesses of 5 mm, 10 mm, and 15 mm, respectively, with an average deviation of 1.66%. For ABS, the corresponding differences were 4.72%, 8.38%, and 12.82%, with an average of 8.64%. At 70 kVp, PLA

Table 2. Comparison of MCNP and experimental penetrated X-ray doses for PMMA, PLA, and ABS at diagnostic tube voltages.

Tube Voltage (kVp)	Thickness (mm)	MCNP			Experiment	
		PMMA	PLA	ABS	PLA	ABS
50	0	289.1	289.1	289.1	289.1	289.1
	5	245.7	248.0	257.3	242.1	257.6
	10	211.0	214.2	228.7	204.1	230.5
	15	182.7	187.3	206.1	172.7	206.4
70	0	606.4	606.4	606.4	606.4	606.4
	5	521.5	534.2	547.0	523.3	551.1
	10	453.6	470.6	495.4	455.5	501.6
	15	397.2	421.4	450.6	398.6	457.2
100	0	1,209	1,209	1,209	1,209	1,209
	5	1,062	1,093	1,110	1,075	1,117
	10	937.0	978.8	1,020	963,7	1,032
	15	836.6	898.3	937.0	863.2	954.7

Table 3. Comparison of simulated X-ray penetration deviation of PLA and ABS relative to PMMA at different tube voltages.

Tube Voltage (kVp)	PLA(%)	ABS(%)
50	1.66	8.64
70	4.10	9.18
100	5.26	8.49
Average	3.67	8.77

showed differences of 2.44%, 3.75%, and 6.11%, averaging 4.10%, while ABS exhibited differences of 4.89%, 9.21%, and 13.45%, with an average of 9.18%. At 100 kVp, the deviations for PLA were 2.96%, 5.43%, and 7.38%, giving an average of 5.26%, whereas ABS presented differences of 4.56%, 8.91%, and 11.99%, with an average of 8.49%. Overall, the mean attenuation differences across all tube voltage conditions were 3.67% for PLA and 8.77% for ABS in Table 3. The close agreement between PLA and PMMA implies that their attenuation behaviors are nearly identical, attributable to the similarity in density and effective atomic number between the two materials. Contrarily, ABS exhibited higher X-ray penetration at the same thickness due to its relatively lower density. Similar findings were reported by Kunert *et al.* (2022), who compared 3D-printed materials with biological tissues and found that ABS most closely represented adipose tissue, while PLA showed the highest similarity to soft tissue [17].

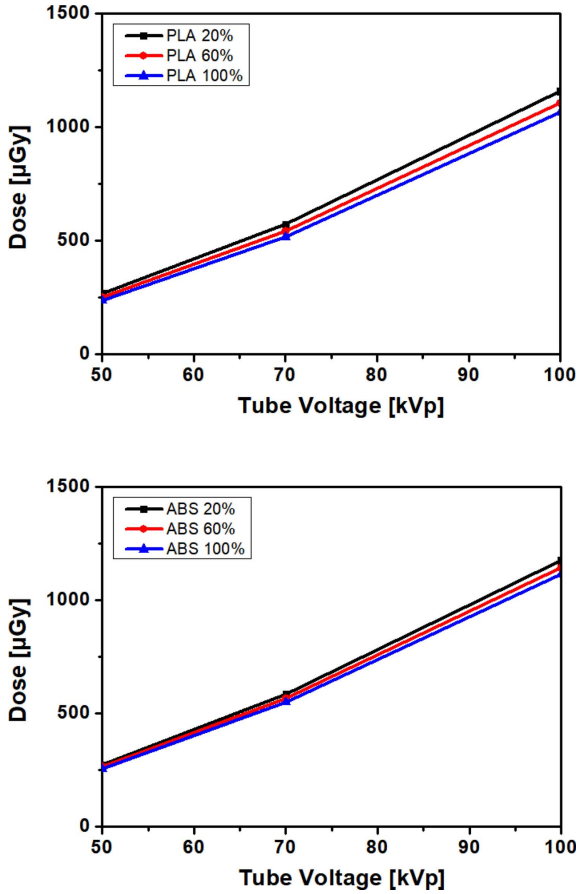

Fig. 5. (Color online) Variation in penetrated X-ray dose for PLA (top) and ABS (bottom) slabs according to tube voltage (50–100 kVp) and infill ratio (20%, 60%, 100%) obtained from MCNP simulations.

The variation in X-ray attenuation according to infill density was analyzed for PLA and ABS slabs with a fixed thickness of 6 mm. As illustrated in Fig. 5, the penetrated dose increased linearly as the infill density decreased at all tube voltages. For PLA, the average difference in penetrated dose between the 100% and 20% infill conditions was 9.88%, and the difference between the 100% and 60% infill conditions was 4.44%. For ABS, the corresponding differences were 5.99% and 2.89%, respectively. These results indicate that the decrease in effective density caused by higher internal porosity directly affects X-ray attenuation. This relationship suggests that internal infill density can serve as a critical parameter in reproducing tissue-equivalent attenuation characteristics of the human body. However, since this study focused on dose-based physical attenuation properties, further research incorporating image-based evaluations is required to achieve a more comprehensive analysis.

4. Conclusion

This study quantitatively evaluated and compared the X-ray attenuation characteristics of 3D-printed thermoplastic materials, PLA and ABS, with those of the conventional phantom material, PMMA, under diagnostic tube voltages of 50 kVp, 70 kVp, and 100 kVp. The average discrepancy between Monte Carlo simulations and experimental measurements was 2.3%, demonstrating the high reliability of the simulation model. PLA demonstrated an average attenuation difference of 3.7% compared to PMMA, indicating nearly identical attenuation behavior. In contrast, ABS exhibited an average difference of 8.8% due to its lower material density. The penetrated dose increased linearly with decreasing infill density, confirming that X-ray attenuation can be effectively controlled by adjusting the effective density. These findings suggest that PLA can be used as a tissue-equivalent phantom material, while ABS may serve as a lightweight or structural support component. The attenuation data for 3D printed materials presented in this study can be directly applied to various clinical and research settings, including QA of diagnostic imaging systems, dose verification phantoms,

and patient-specific calibration phantoms. Future work is expected to focus on optimizing printing parameters and material combinations to develop integrated validation phantoms applicable to multimodality imaging systems, such as CT, MRI, and ultrasound. This approach is expected to enhance the clinical applicability and industrial scalability of 3D printing-based medical phantoms.

References

[1] M. Amurao, E. Samei, M. Flynn, L. M. Klem, A. M. Reilly, and D. L. Jordan, J. Appl. Clin. Med. Phys. **24**, e13885 (2023).
[2] T. Khinvasara, S. Ness, and A. Shankar, Asian J. Res. Comput. Sci. **17**, 13 (2024).
[3] K. E. Keenan, K. V. Jordanova, S. E. Ogier, D. Tamada, N. Bruhwiler, J. Starekova, J. Riek, P. J. McCracken, and D. Hernando, Magn. Reson. Mater. Phys. Biol. Med. **37**, 535 (2024).
[4] S. Widodo and K. Brazovskiy, J. Phys.: Conf. Ser. **2945**, 012013 (2025).
[5] M. Alzahrani, D. A. Broadbent, I. Teh, B. Al-Qaisieh, E. Johnstone, and R. Speight, Phys. Imaging Radiat. Oncol. **37**, 535 (2025).
[6] H. Yusuff, P.-E. Zorn, C. Giraudeau, B. Wach, P. Choquet, S. Chatelin, and J.-P. Dillenseger, Magn. Reson. Mater. Phys. Biol. Med. **38**, 561 (2025).
[7] M. Alzahrani, D. A. Broadbent, I. Teh, B. Al-Qaisieh, and R. Speight, Phys. Med. Biol. **69**, 215034 (2024).
[8] M. Wegner and D. Krause, J. Mech. Sci. Technol. **38**, 4537 (2024).
[9] A. R. Khoshhal and A. Esmaili Torshabi, J. Nucl. Res. Appl. **4**, 24 (2024).
[10] S. Hatamikia, L. Jaksa, G. Kronreif, W. Birkfellner, J. Kettenbach, M. Buschmann, and A. Lorenz, Z. Med. Phys. **35**, 138 (2025).
[11] J. Qiu, K. Hou, B. A. Dyer, J.-C. Chen, L. Shi, Y. Sun, L. Xu, H. Zhao, Z. Li, T. Chen, M. Li, F. Zhang, H. Zhang, and Y. Rong, Front. Phys. **9**, 605630 (2021).
[12] P. Kunert, H. Schlattl, S. Trinkl, E. Honorio da Silva, D. Reichert, and A. Giussani, Med. Phys. **51**, 9264 (2024).
[13] I. Ozsoykal and A. Yurt, Appl. Sci. **14**, 509 (2024).
[14] Los Alamos National Laboratory (LANL), MCNP® Code Version 6.3.1 Release Notes, LA-UR-25-23548-Rev. 1, Los Alamos, NM (2025).
[15] Institute of Physics and Engineering in Medicine (IPEM), Report 78: Catalogue of Diagnostic X-Ray Spectra and Other Data (1997).
[16] National Bureau of Standards (NBS), XCOM: Photon Cross Sections on a Personal Computer, NBSIR-87-3597, Washington, DC (1987).
[17] P. Kunert, S. Trinkl, A. Giussani, D. Reichert, and G. Brix, Med. Phys. **49**, 7766 (2022).